J Nanostruct 13(2): 530-543, Spring 2023

RESEARCH PAPER

Ampicillin and Ibuprofen Removal from Aqueous Solution by a Facil and Eco-Friendly Synthesis of Silver Nanoparticles Using Thymus Fedtschenkoi Leaves: Isotherm and Kinetic Studies

Robab Lotfollahzadeh [1], Mohammad Yari [1], Sajjad Sedaghat [2], Akram Sadat Delbari [1]*

[1] Department of Chemistry, College of Science, Islamshahr Branch, Islamic Azad University, Islamshahr, Iran

[2] Department of Chemistry, College of Science, Shahr-e-Qods Branch, Islamic Azad University, Shahr-e-Qods, Iran

ARTICLE INFO

Article History:
Received 11 November 2022
Accepted 19 March 2023
Published 01 April 2023

Keywords:
Adsorption
Ampicillin
Green synthesis
Ibuprofen
Silver nanoparticles
Thymus fedtschenkoi

ABSTRACT

This study reports the removal of Ampicillin (AMP) and Ibuprofen (IBU) using synthesized silver nanoparticles (AgNPs) from *Thymus fedtschenkoi* leaves. This adsorbent was characterized by scanning electron microscope (SEM), transmission electron microscopy (TEM), energy-dispersive X-ray analysis (EDX), Fourier-transform infrared spectroscopy (FTIR), and X-ray powder diffraction (XRD) techniques. The maximum removal efficiency was found at pH=4 (AMP) and pH=6 (IBU), the contact time=30 min, the adsorbent dosage=0.5 g, and drug concentration=30 mg/L. The Langmuir and Freundlich isotherms were investigated to show the adsorption behavior of AMP and IBU. The adsorption data followed the Langmuir model with coefficient of determination (R^2)> 0.99. The maximum adsorption capacity (q_{max}) was obtained 31.84 and 27.17 mg g^{-1} for AMP and IBU, respectively. Also, kinetic studies revealed that adsorption of AMP and IBU were fitted to the pseudo-second-order model with R^2 higher than 0.98. AgNPs from *Thymus fedtschenkoi* can be a promising, inexpensive, and green adsorbent.

How to cite this article
Lotfollahzadeh R, Yari M, Sedaghat S, Delbari A. Ampicillin and Ibuprofen Removal from Aqueous Solution by a Facil and Eco-Friendly Synthesis of Silver Nanoparticles Using Thymus Fedtschenkoi Leaves: Isotherm and Kinetic Studies. J Nanostruct, 2023; 13(2):530-543. DOI: 10.22052/JNS.2023.02.023

INTRODUCTION

In developing countries, the lack of water with good quality is a main environmental issue. The reason for this problem is the discharge of effluents from various factories into the aquatic media, which is increasing daily. These industries include pharmaceuticals, textiles, and cosmetics, which have a role in water contamination via the discharge of wastewater produced from their activities [1]. Wastewaters related to the pharmaceutical are very hazardous and toxic for both human and environmental life [2]. Indeed, there are pharmaceutical components as residues in water and have been considered as part of the hazardous chemical materials, which can change the natural balance system of the surrounding environment [3].

One of the emerging contaminants is antibiotics drugs, which exists in different water media. These groups are prescribed to treat the infection in humans and animals. Municipal, hospital, and pharmaceutical factories wastewaters are the main production antibiotics sources in the aqueous medium [4]. One of the broadest groups of antibiotics is -lactam that ampicillin (AMP) (Fig.

* Corresponding Author Email: yari.mohammad55@yahoo.com

Table 1. Abbreviations used in the text

Abbreviation	Explanation
AMP	Ampicillin
IBU	Ibuprofen
AgNPs	Silver nanoparticles
SEM	Scanning electron microscope
TEM	Transmission electron microscopy
EDX	Energy-dispersive X-ray analysis
FTIR	Fourier-transform infrared spectroscopy
XRD	X-ray powder diffraction
q_{max}	Maximum adsorption capacity
NSAIDs	Non-steroidal anti-inflammatory drugs
DBD	Dielectric barrier discharge

1) belongs to this category. Excretion of oral and intravenous AMP is 30% and 75%, respectively. Antibiotics and their metabolites in aqueous environment lead to an increase in antibiotic-resistant bacteria or pathogens [5]. Therefore, the removal of antibiotics from aqueous solutions before release into the aquatic ecosystem is very necessary [6].

The other drugs that extensively used for treating diseases related to the human and animal are non-steroidal anti-inflammatory drugs (NSAIDs). This pharmaceutical group has antipyretic, analgesic, and anti-inflammatory properties. The increasing use of these drugs causes entry into the aqueous environment, which endangers the health of aquatic animals, humans, and animals. One of the most widely used NSAIDs is ibuprofen (IBU) (Fig. 2) [7]. Fever symptoms, headaches, arthritis, menstrual cramps, and other usual pains can be relieved by IBU [8]. In one research, an excretion of 85% of ingested IBU through urine was reported, which is not totally metabolized and enters the environment [9].

There are various technologies such as electrochemistry [10], oxidation [11-13], dielectric barrier discharge (DBD) [14], Fenton and photo-Fenton [15], adsorption [16-18] have been used for the removal of AMP, IBU, and other pollutants. Among these methods, adsorption has become more attractive owing to its low cost, high efficiency, ability to regenerate, and environmentally-friendly nature [19]. A number of adsorbents have been applied to adsorb AMP and IBU such as activated carbon [20], graphene oxide nanoplatelets [21], zeolite-rich composite [22], and so on.

The nanotechnology field has made significant progress due to the notable features related to the nanoscale materials. Silver and gold nanoparticles (NPs) possess unique characteristics with convenient pliability [23,24]. Silver nanoparticles (AgNPs) are specified by their anti-bacterial nature and facile separation. In addition, catalytic activity, a relatively high adsorption capacity and high surface area for their small size are the other positive properties related to these NPs. Their applications are in food production, clothing industry, household products, cosmetics, wound dressings, biomedical, as well as water and air purification [25]. Also, AgNPs can strongly absorb visible light due to their localized surface plasmon resonance (LSPR). This property of AgNPs has gained remarkable interest in various fields such as medicine, near-field optics, surface-enhanced spectroscopy, and solar cells [26]. AgNPs have attained more significance in the field of water treatment owing to physicochemical features [27,28].

There are many approaches such as photochemical, physical, and chemical for the synthesis of AgNPs [29]. In most of these synthesis methods, hazardous chemicals such as hydrazine (N_2H_4), sodium borohydride ($NaBH_4$), N,N-dimethylformamide (C_3H_7NO), sodium sulfide (Na_2S), and surfactants used as reducing agents for converting Ag ions into Ag element, which are harmful to living organisms and the environment [23,30]. Biological synthesis of NPs is the other

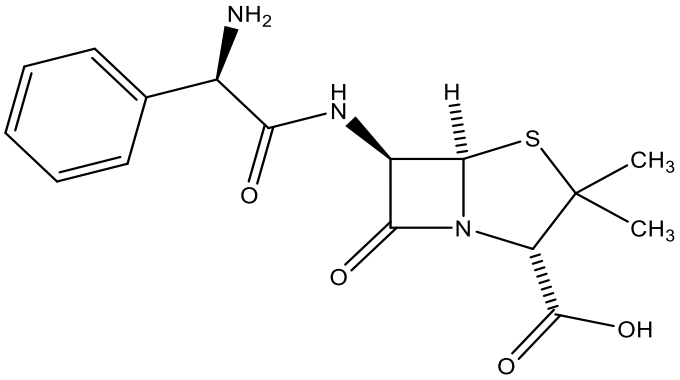

Fig. 1. Chemical structure of AMP.

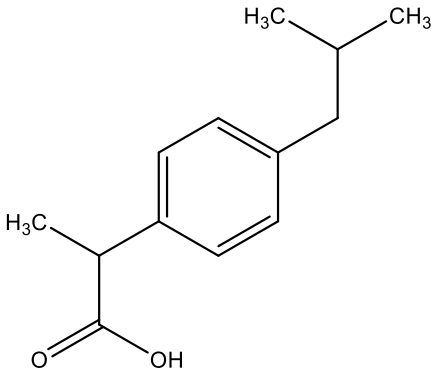

Fig. 2. Chemical structure of IBU.

method, which use marine algae, microorganisms, fruits, whole plants, plant tissue, and plant extract as reducing agents. This kind of synthesis can decrease the environmental effect and make large amounts of NPs without pollution with a certain size and morphology [31]. Plant extracts are known as the best biological substances due to their abundance and their compounds as reducing agents for facilitating the formation of NPs. Also, the process of AgNPs production using plants is quick, single step, inexpensive, and eco-friendly [25,32].

Thymus is called "Avishan" in Persian, and belongs to Lamiaceae family, which is known as aromatic and medicinal plant. This plant grows in West Asia, North-West of Grönland Island, North Africa, and Mediterranean area to Europe. Antibacterial, antiviral, antifungal, antioxidant, and antiparasitic are the strong activities of *Thymus* species. There are 14 species of this genus in Iran. One of the semi endemic plants of Iran is *Thymus fedtschenkoi*, which distributes naturally in some parts of Turkey and the Caucasus [33-35].

In this study, the *Thymus fedtschenkoi* extract was used to synthesize AgNPs for removing AMP and IBU from aqueous solution. For the first time, this biosynthesis was implemented to eliminate drug contaminants. Synthesized NPs were characterized using scanning electron microscope (SEM), transmission electron microscopy (TEM), energy-dispersive X-ray analysis (EDX), Fourier-transform infrared spectroscopy (FTIR), and X-ray powder diffraction (XRD). Experimental parameters, including pH, contact time, adsorbent dosage, and drug concentration were investigated and optimized values were selected.

MATERIALS AND METHODS

Chemicals

Silver nitrate (99.9%), AMP, and IBU were procured from Jaber Ebne Hayyan pharmaceutical company. *Thymus fedtschenkoi* leaves were provided from Mianeh city, East Azerbaijan, Tabriz, Iran.

Apparatus

Absorption spectra related to the solutions were recorded using a UV-Vis spectrophotometer (Shimadzu, Japan, UV-1800). Formation and surface morphology of AgNPs were evaluated by SEM (TSCAN company, Czech), Sigma VP-500 equipped with an EDX detector (LEO 9121413). TEM (Zeiss company, Germany, EM 10C-1000Kv) was applied to measure the size of AgNPs. FTIR was used to determine the functional groups of plant and AgNPs between 400 and 4000 cm^{-1} at a resolution of 4 cm^{-1}, by averaging 32 scans (PerkinElmer Spectrum 100 FTIR). The crystalline structure of AgNPs was characterized by the XRD (Malvern Panalytical company, United Kingdom) using a Bragg–Brentano geometry, equipped with a Cu anode (λCuKα = 1.54184 Å) X-ray tube and hybrid monochromator (Ge220). The XRD was obtained in the 2θ range 7.05–79.95°. An acquisition step of 0.02° and an acquisition time of 10s per step were used. Elemental analysis was carried out using EDX (Czech Republic, MIRA III).

Preparation of plant water extract

The leaves of the *Thymus fedtschenkoi* plant were collected and washed with water. Then, drying these leaves were done at room temperature for 5 days. All leaves were completely powdered. Afterward, 100 mL of double-distilled water and 7 g of powdered leaves were mixed

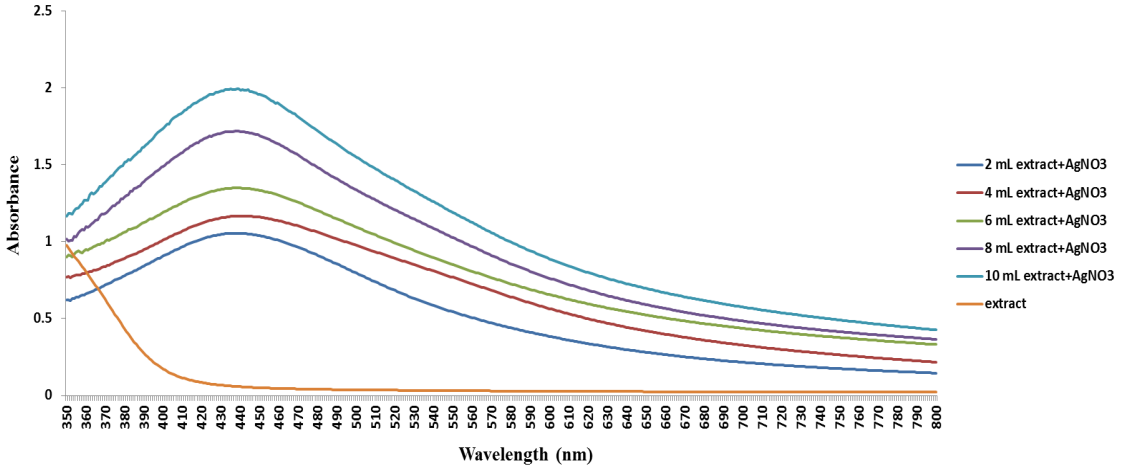

(a)

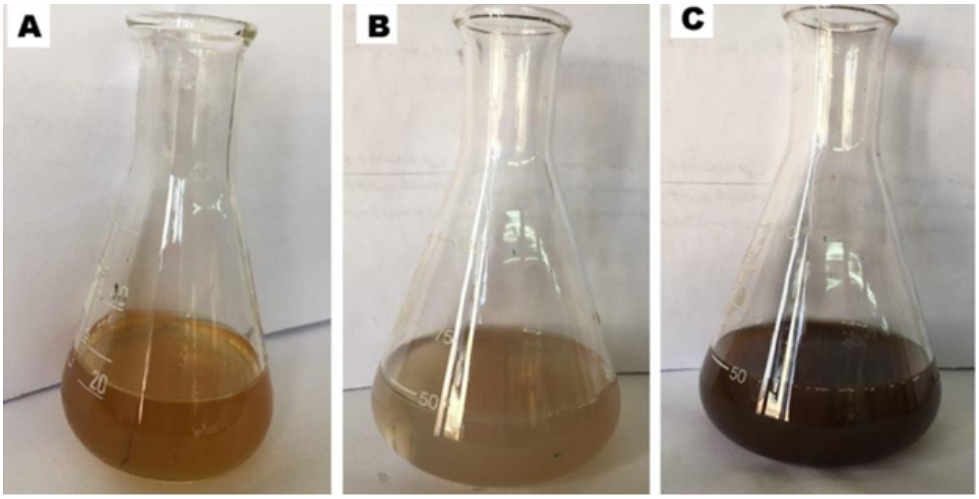

(b)

Fig. 3. (a) UV–Vis spectra of different concentrations of plant extract and (b) color change of solution during the reaction.

together, and boiling was performed at 60 ºC for 20 min. Whatman paper No.14 was used to filter this solution. Finally, it was stored in a dark bottle and refrigerator for the next steps.

Synthesis of AgNPs

10 mL of *Thymus fedtschenkoi* extract was poured dropwise into the Erlenmeyer flask containing 100 mL of $AgNO_3$ (0.01 M) and stirred by 500 rpm at 25 ºC for 24 h. Color solution was changed from yellowish-brown to dark brown, which represented the AgNPs formation. Then, the centrifuge was accomplished at a rate of 5000 rpm for 20 min. Eventually, the obtained AgNPs were dried at 70 ºC for 5 h.

Drug removal

Various concentrations of AMP and IBU (30, 40, 50 mg/L) was separately mixed with 0.5 g AgNPs. Sampling was implemented at the time of 5 to 45 min. Also, pH range was considered between 2 to 10. Absorption spectra related to the AMP and IBU were recorded by UV-Vis spectrophotometer. Eq (1) was used to calculate the percentage of AMP and IBU from aqueous solution.

$$Removal\ (\%) = \frac{C_0 - C_e}{C_0} \times 100 \qquad (1)$$

In this equation, the drug initial and final concentration (mg/L) was denoted by C_0 and C_e, respectively [36].

RESULTS AND DISCUSSION

Characterization

UV-Vis spectra

UV-Vis spectrophotometry was used to assess the size and shape of AgNPs in aqueous solutions. Various volumes of plant extract (2, 4, 6, 8, 10 mL) were individually added in the different concentration of $AgNO_3$ solution with a volume of 100 mL. Different reaction times (1, 2, 4, 12, and 24 h) were considered. Recording the absorption spectra was in the range of 350 to 800 (Fig 3a). The broad spectra (380 to 480 nm) in Fig. 3 are corresponding to the decrease of AgNPs size [37]. The reaction was performed between $AgNO_3$ and extract and changing solution color from yellowish-brown to dark brown occurred (Fig 3b). This is related to the surface plasmon resonance (SPR) feature of AgNPs.

SEM analysis

The surface morphology of the synthesized AgNPs was investigated using SEM (Fig. 4). The formation of spherical AgNPs confirmed the AgNPs were well synthesized using *Thymus fedtschenkoi*. The particles are clustered together in the form of small spheres. This agglomeration may be due to the presence of other elements as shown in the EDX spectrum. The particle size varies from 41.80

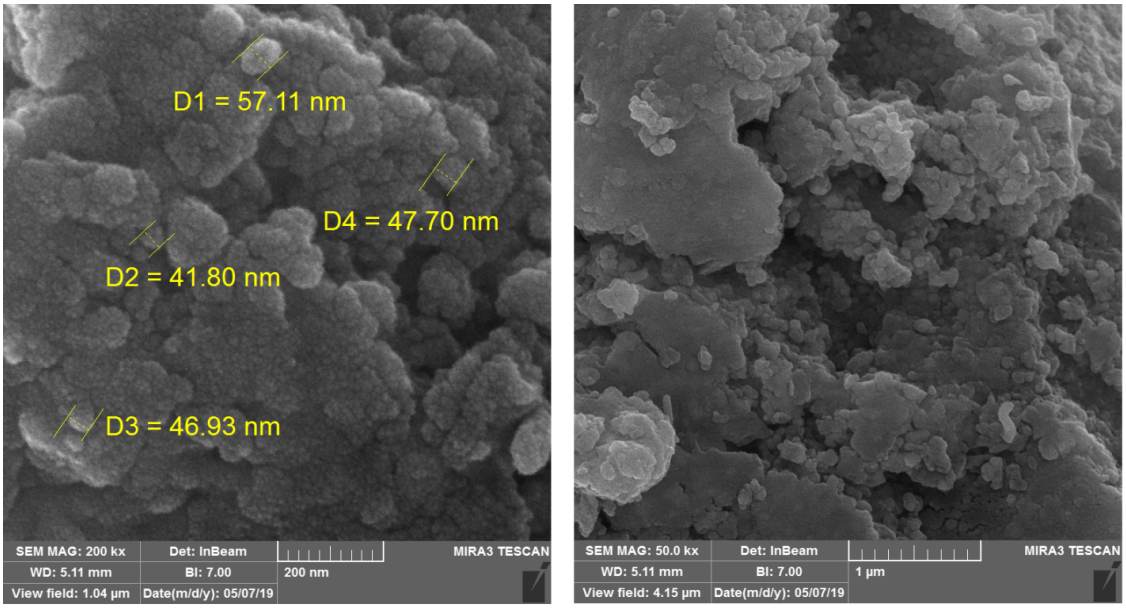

Fig. 4. SEM image of synthesized AgNPs using *Thymus fedtschenkoi.*

nm to 57.11 nm. Benakashani et al. showed the synthesized AgNPs with a green synthesis that they were well dispersed with a spherical shape. These particle sizes were in the range of 10 to 40 nm [38]. Hamelian et al. indicated the SEM of synthesized AgNPs using Thymus Kotschyanus, which denoted the spherical shape with the size of 50 to 60 nm [39].

TEM analysis

In order to determine the size and morphology of the biosynthesized AgNPs, TEM was used (Fig. 5a). It can be concluded that the AgNPs are spherically in shape, and they have a non-uniform distribution. The particle size distribution of AgNPs revealed that the mean size of NPs was 8.6 nm (Fig. 5b). Hamelian et al. revealed the TEM image of AgNPs with an almost spherical shape without agglomeration [39]. In the other literature, the TEM image of synthesized AgNPs using a medicinal plant has been indicated. The spherical shape and size range between 7 to 32 nm have been reported [40].

FTIR analysis

Fig. 6 illustrates the FTIR spectra of the leaf extract and biosynthesized AgNPs. The presence of diverse functional groups is shown in these spectra. The broad peak at 3389 cm^{-1} represents the stretching vibration of the OH or NH groups

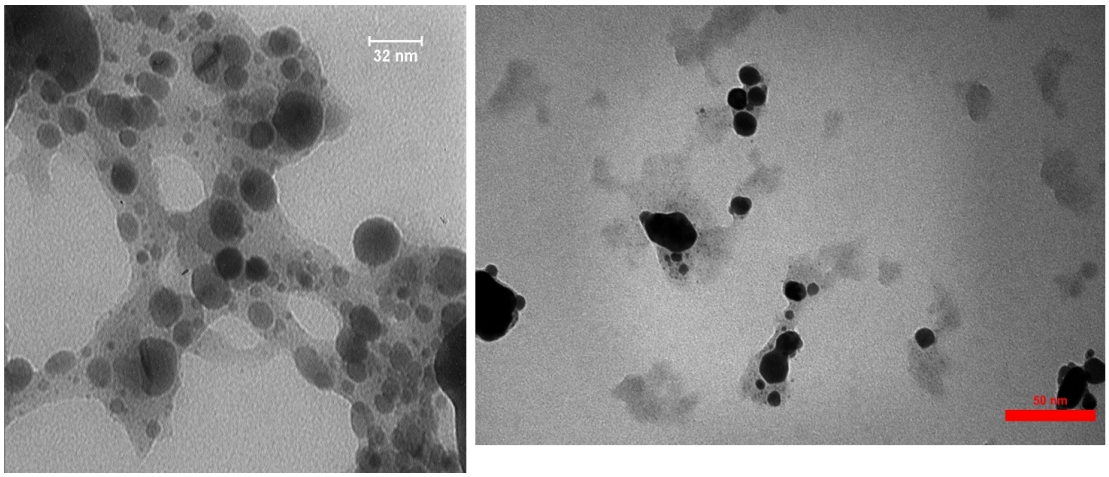

(a)

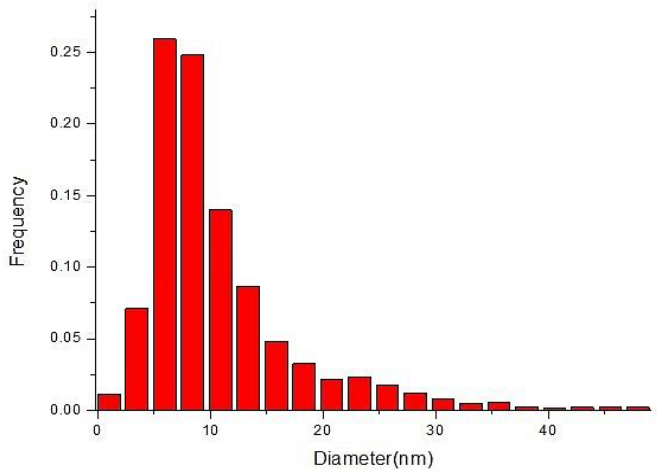

(b)

Fig. 5. (a) TEM image and (b) histogram of obtained AgNPs.

of phenolic compounds present in the leaf extract. The peak at 2353 cm^{-1} is related to the C=O stretching vibration. The band at 1605 cm^{-1} is due to the C=C stretching of alkenyl or aromatic. The absorption peak at 1409 cm^{-1} is related to the stretching of the CO group. The observed band at 1060 cm^{-1} is attributed to CN stretching [38, 39, 41].

XRD analysis

The crystal structure of synthesized AgNPs was performed using XRD analysis (Fig. 7). Observed peaks at 2θ=28, 32, 38, 44, 46, 55, 57, 64, and 77 is assigned to the 111, 200, 111, 200, 220, 311, 222, 220, and 311 planes, respectively. The XRD pattern was matched with the joint committee on powder diffraction standards (JCPDS) file No. 01-071-4613.

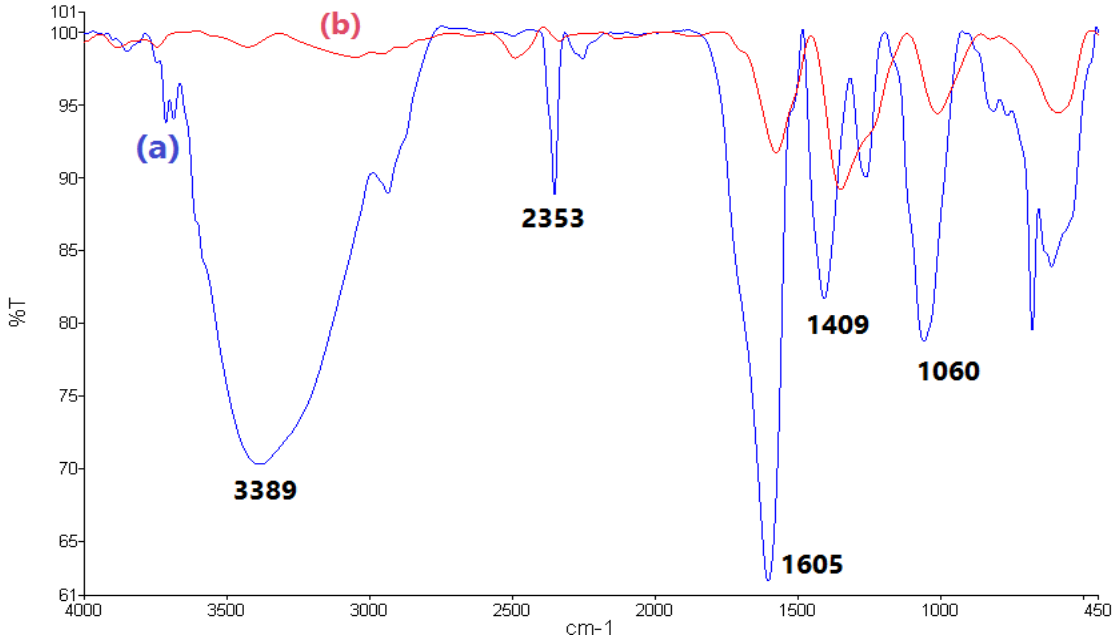

Fig. 6. FTIR spectra of (a) *Thymus fedtschenkoi* extract and (b) AgNPs synthesized using *Thymus fedtschenkoi.*

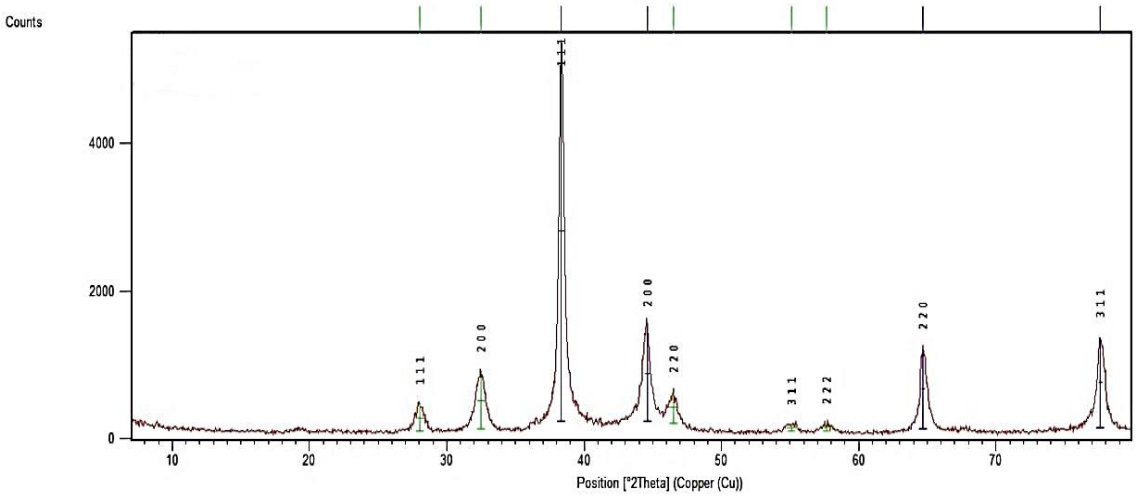

Fig. 7. XRD pattern of synthesized AgNPs using *Thymus fedtschenkoi.*

Crystallite size of AgNPs was calculated by Debye-Scherrer formula (Eq 2).

$$D = \frac{K\lambda}{\beta cos\theta} \quad (2)$$

Herein D shows the crystalline size of NPs, K denotes the Scherer constant (between 0.9 to 1), , , and are the wavelength of the X-ray source, the full width at the half maximum related to the diffraction peak, and the Bragg's angle, respectively [38]. According to this equation, the average particle size was achieved 24 nm.

EDX analysis

As shown in Fig. 8, confirmation of elemental analysis of AgNPs was implemented by EDX. A strong signal of the peak (84.41%) was at 3 KeV is related to the absorption of metallic AgNPs. The presence of very small amounts of other elements indicates the relatively good purity of the nanoparticles.

AgNPs synthesis mechanism by plant extract

Trapping of silver ions on the surface of plant proteins occurs due to the electrostatic interaction between them. Plant proteins reduces silver ions, which leads to the formation of silver nuclei. According to the reduction process, these nuclei grow continuously. The formation of AgNPs occurs due to the accumulation of these nuclei [42].

Optimization

The effect of the pH

The influence of pH on the elimination of AMP and IBU was surveyed over the pH range 2–10. As seen in Fig. 9a, AMX and IBU drugs were strongly adsorbed on the AgNps at the pH of 4 and 6, respectively. At these pH, the removal of AMP and IBU was the highest with reaching 95.78 and 94.13%, respectively. The removal of AMP was diminished at pH values less than 4 and above 6, which is due to the effect of pH on AMP ionized species, the charging of the adsorbent surface, and the interactions between them. AMP has an amphoteric feature, which shows two dissociation constants: pKa_1=2.77 and pKa_2=7.14. The AMP carries positive and negative charges at pH=2.77 and above pH=7.14, respectively. There is a zwitterionic structure with pK_a values between 2.77 to 7.14. An anionic structure can be observed at pH above 7.14. By increasing pH, COOH group will be converted to COO^-. Hence, the repulsion between AMP and adsorbent would increase, which lead to decrease the removal efficiency. The best removal was achieved at pH=4 (95.78%) [43,44].

About removing IBU, under conditions of pH< pH_{pzc}, the adsorbent surface has positive charge, as well as under strongly acidic conditions, the carboxylic acid (COOH) group of the IBU is protonated and not charged. So, at the pH of 4 and 6, the transition from neutral protonated to negatively charged deprotonated occurs in the COOH group. The negative charges of the COOH group interact with the positive charge of the adsorbent and make the electrostatic interaction. The pK_a value related to the COOH group of IBU is 4.35. In pH>pH_{pzc}, both drug and adsorbent

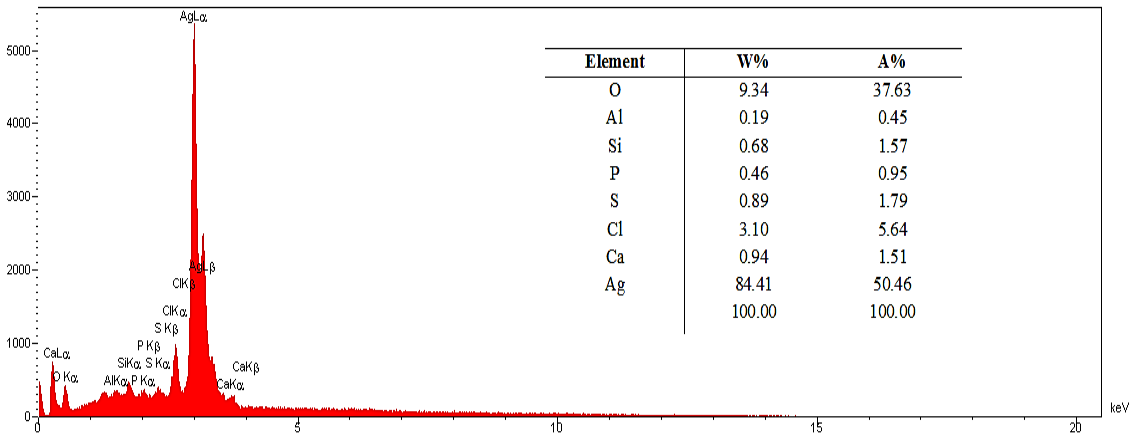

Element	W%	A%
O	9.34	37.63
Al	0.19	0.45
Si	0.68	1.57
P	0.46	0.95
S	0.89	1.79
Cl	3.10	5.64
Ca	0.94	1.51
Ag	84.41	50.46
	100.00	100.00

Fig. 8. EDX spectrum of synthesized AgNPs using *Thymus fedtschenkoi.*

possess negative charges. Hence, at higher values of pH, the removal becomes decreased owing to the increasing electrostatic repulsions [45]. Finally, the pH value of 6 was chosen for further experiments.

The effect of contact time

The influence of contact time from 5 to 45 min on the AMP and IBU adsorption was evaluated. According to Fig. 9b, the AMP and IBU removal rate was increased to 30 min. It can be concluded that at initial times all active sites related to the adsorbent surface are available. By decreasing available sites, the system was reached an equilibrium state. From 30 to 45 min, the percentage removal was increased from 95.88 to 96.59% and 94.25 to 95.22% for AMP and IBU, respectively. There was no significant difference between 30 and 45 min. Thus, the contact time of 30 min was considered for this process [43].

The effect of adsorbent dosage

In order to obtain a quantitative adsorption of the drugs and to reduce the costs corresponding to the adsorption, the effect of adsorbent dose is a significant factor. Different amounts of AgNPs (between 0.1 and 0.5 g) were tested. By increasing the adsorbent dose from 0.1 to 0.5 g, the removal percentage of the AMP and IBU was increased owing to the increase in the specific surface area and the presence of several active adsorption sites (Fig. 9c). This is mainly ascribed to the effect of the interactions between the particles, such as aggregation leading to an increase in diffusion path length and a decrease in total surface area of the adsorbent [46].

The effect of initial concentration

The effect of this factor was studied on the removal efficiency by changing the initial concentration of AMP and IBU (30, 40, 50 mg/L) (Fig. 9d). The removal percentage of both drugs declined when the initial concentration of AMP and IBU increased. This is probably owing to an increase in the driving force of the concentration gradient, as an increase in the initial AMP and IBU concentration. This is due to more pore available on the adsorbent surface in low concentration. When the surface active sites of the adsorbent are covered fully, the extent of adsorption reaches a

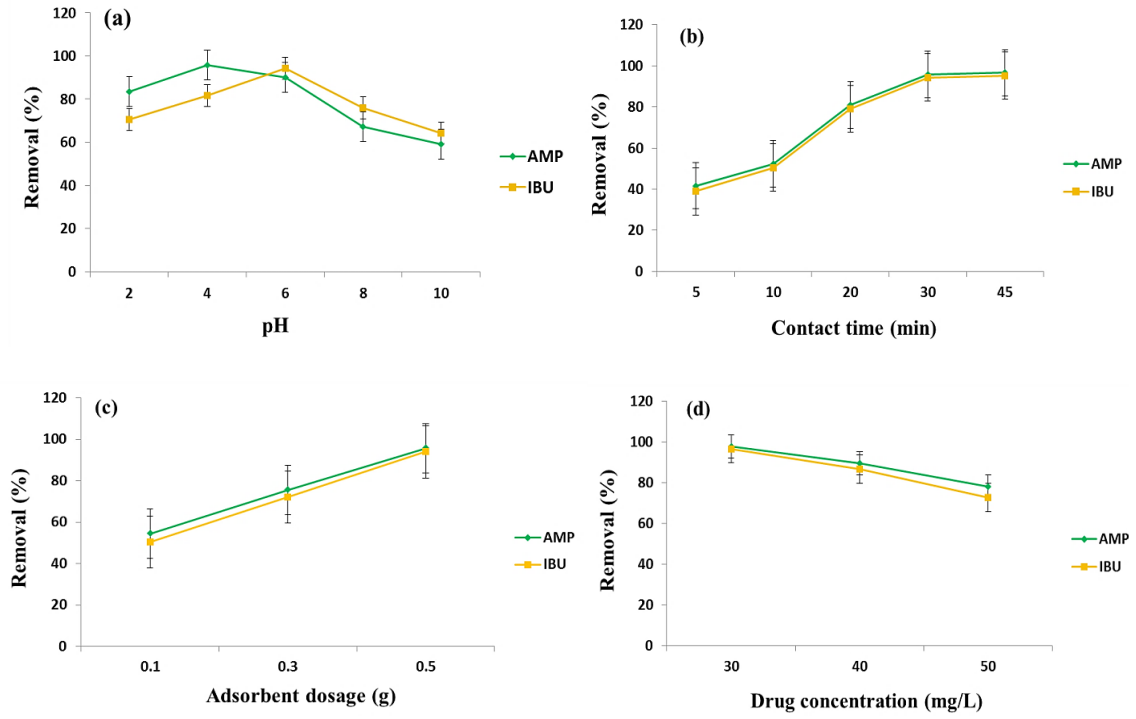

Fig. 9. The effect of (a) pH, (b) contact time, (c) adsorbent dosage, and (d) initial concentration of drug for the removal of AMP and IBU.

limit resulting in saturated adsorption.

Adsorption isotherms

The basis of the Langmuir isotherm is monolayer adsorption. Indeed, the formation of a layer on the surface of the adsorbent using molecules of dissolved components is observed. Regarding this model, the nanoadsorbent surface is assumed homogeneous [47]. The Langmuir model is described via Eq (3).

$$\frac{C_e}{q_e} = \frac{1}{q_m K_L} + \frac{1}{q_m} C_e \quad (3)$$

Herein, the q_e and C_e express the adsorption capacity and drug concentration at equilibrium, respectively. The maximum adsorption capacity and Langmuir constant are denoted by q_{max} and K_L. By plotting C_e/q_e against C_e, these values were obtained (Fig. 10a).

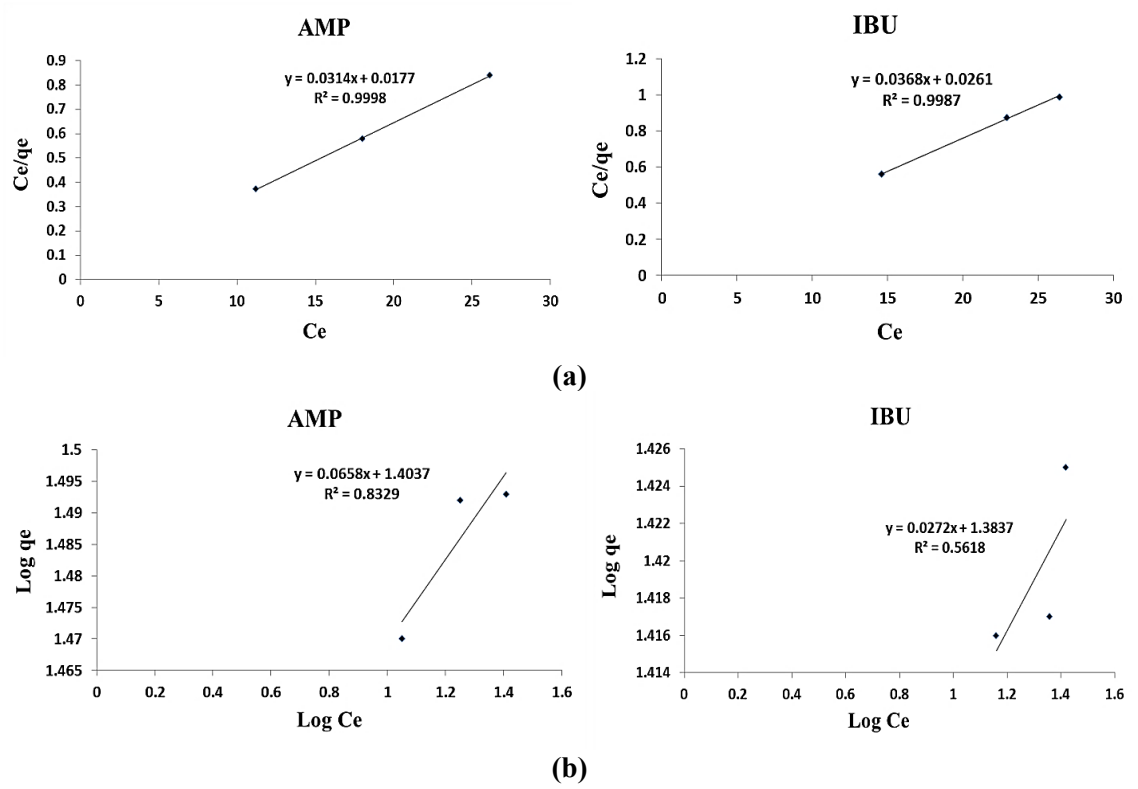

Fig. 10. (a) Langmuir and (b) Freundlich isotherms for the removal of AMP and IBU by synthesized AgNPs.

Table 2. The obtained parameters of isotherm models for AMP and IBU removal.

		Contaminant	
Isotherms	Parameters	AMP	IBU
Langmuir	q_{max} (mg/g)	31.84	27.17
	K_L (L/mg)	1.774	1.410
	R^2	0.9998	0.9987
Freundlich	K_f (mg/g)	25.33	24.19
	1/n	0.0658	0.0272
	R^2	0.8329	0.5618

In the Freundlich isotherm, the nanoadsorbent surface and adsorption are considered heterogeneous and multilayer, respectively. The linear form of this model is represented by Eq (4).

$$Log\ q_e = log\ (K_f) + \frac{1}{n}\ log\ (C_e) \quad (4)$$

Where, the Freundlich constant and adsorption intensity are shown by K_F and 1/n, respectively. The value of n determines the nature of the adsorption. When n=1, n<1, and n >1, the adsorption is linear, chemical, and physical, respectively. The values of 1/n and K_F are achieved by plotting log q_e versus log C_e (Fig. 10b) [48].

The isotherm parameters corresponding to the mentioned models were calculated and given in Table 2. The results indicated that the data fitted well within the Langmuir isotherm. This was assigned to the higher value of the coefficient of determination (R^2) related to this isotherm, which

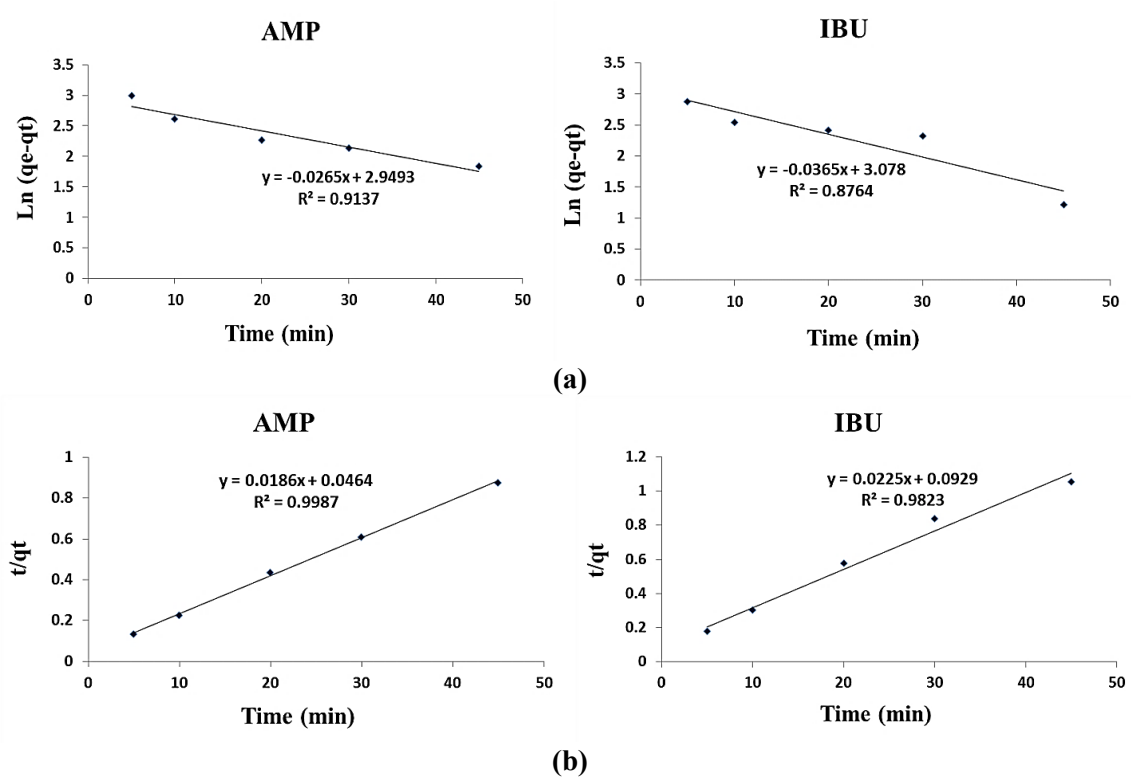

Fig. 11. (a) Pseudo first-order and (b) Pseudo second-order adsorption kinetics of AMP and IBU.

Table 3. The obtained kinetic parameters for AMP and IBU removal.

		Contaminant	
Kinetic	Parameters	AMP	IBU
Pseudo-first-order	K_1 (min^{-1})	0.0265	0.0365
	q_e (mg g^{-1})	19.09	21.71
	R^2	0.9137	0.8764
Pseudo-second-order	K_2 ($g.mg^{-1}.\ min^{-1}$)	7.45×10^{-3}	5.45×10^{-3}
	q_e (mg g^{-1})	53.76	44.44
	R^2	0.9987	0.9823

Table 4. Comparison of various studies for the removal of AMP and IBU.

Adsorbent	Pollutant	q_{max} (mg/g)	Removal efficiency (%)	Time (min)	Ref.
CNT-COOH/MnO_2/Fe_3O_4	IBU	103.09	94.00	20	[46]
Activated carbon	AMP	12.7	73.00	120	[33]
$CoFe_2O_4$[1]	AMP	---	90.00	25	[17]
Calcite sludge-aluminum hydroxide	IBU	34.96	---	---	[52]
Activated carbon from Oak Acorn	IBU	96.15	---	120	[53]
AgNPs	AMX	31.84	95.88	30	Present study
AgNPs	IBU	27.17	94.25	30	Present study

[1]Cobalt Ferrite nanoparticles

was equal to 0.9998 and 0.9987 for AMP and IBU, respectively. The results confirmed that the adsorption was a monolayer process.

Adsorption kinetics

Adsorption kinetics can describe the adsorption rate and process mechanism control. The pseudo-first order model was used in the form of Ho and McKay equation.

$$ln\,(q_e - q_t) = lnq_e - k_1(t) \quad (5)$$

The linear form of pseudo-second order model is described in Eq (6).

$$\frac{t}{q_t} = \frac{1}{k_2 q_e^2} + \frac{t}{q_e} \quad (6)$$

Herein, q_e and q_t (mg g^{-1}) denote the value of AMP and IBU adsorbed at equilibrium and time t, respectively. The pseudo-first order and pseudo-second order rate constant are shown by k_1 and k_2, respectively [49,50]. Linear plots were drawn based on the mentioned kinetic models (Fig. 11). It is clear that the R^2 values of pseudo second-order related to the both drugs were higher than the other model. The calculated adsorption capacity ($q_{e,cal}$) by the pseudo second-order model was 53.76 and 44.44 mg g^{-1} for AMP and IBU, respectively (Table 3).

Comparison of adsorption capacity with various adsorbents

The adsorption capacity of various adsorbents for the removal of AMP and IBP from aqueous solutions is given in Table 4. It can be stated that AgNPs derived from *Thymus fedtschenkoi* can be used as an alternative adsorbent for the removal of these drugs with minimum time (30 min) and high removal percentage and proper maximum adsorption capacity. For the first time, green synthesis of AgNPs was performed using *Thymus fedtschenkoi* plant for the removal of IBU and AMX. Easier, more environmentally friendly synthesis and proper performance along with economics are other outstanding features of this adsorbent compared to other adsorbents. In some studies, the application of AgNPs was investigated in terms of antimicrobial activity [51]. While this property has not been evaluated in this work.

CONCLUSION

In summary, a facile, cost effective, and green method was demonstrated for the synthesis of AgNPs from *Thymus fedtschenkoi* for the removal of antibiotic and anti-inflammatory drugs. The prepared AgNPs was characterized by SEM, TEM, FTIR, XRD, and EDX techniques. The effects of various experimental parameters such as pH, contact time, adsorbent dose, and pollutant concentration were examined on the value of adsorption. The behavior of adsorption related to the AMP and IBU was considered by the Langmuir and Freundlich isotherm models and the maximum adsorption capacity of adsorbent for the removal of these drugs was calculated. Also, the adsorption kinetics data were fitted to the pseudo-second-order. Compared with physical and chemical synthesis methods, the green synthesis of AgNPs is a more cost-effective and nature-friendly procedure for pollutant treatment. Furthermore, it can be an efficient alternative adsorbent for the removal of AMP and IBU from aqueous media.

CONFLICT OF INTEREST

The authors declare that there is no conflict of interests regarding the publication of this manuscript.

REFERENCES

1. Bello OS, Moshood MA, Ewetumo BA, Afolabi IC. Ibuprofen removal using coconut husk activated Biomass. Chemical Data Collections. 2020;29:100533.

2. Martín J, Orta MdM, Medina-Carrasco S, Santos JL, Aparicio I, Alonso E. Evaluation of a modified mica and montmorillonite for the adsorption of ibuprofen from aqueous media. Applied Clay Science. 2019;171:29-37.
3. Ghauch A, Tuqan A, Assi HA. Antibiotic removal from water: Elimination of amoxicillin and ampicillin by microscale and nanoscale iron particles. Environ Pollut. 2009;157(5):1626-1635.
4. Rahman N, Varshney P. Assessment of ampicillin removal efficiency from aqueous solution by polydopamine/zirconium(iv) iodate: optimization by response surface methodology. RSC Advances. 2020;10(34):20322-20337.
5. Mirzaei A, Haghighat F, Chen Z, Yerushalmi L. Sonocatalytic removal of ampicillin by Zn(OH)F: Effect of operating parameters, toxicological evaluation and by-products identification. J Hazard Mater. 2019;375:86-95.
6. Montoya-Rodríguez DM, Serna-Galvis EA, Ferraro F, Torres-Palma RA. Degradation of the emerging concern pollutant ampicillin in aqueous media by sonochemical advanced oxidation processes - Parameters effect, removal of antimicrobial activity and pollutant treatment in hydrolyzed urine. J Environ Manage. 2020;261:110224.
7. Ghemit R, Makhloufi A, Djebri N, Flilissa A, Zerroual L, Boutahala M. Adsorptive removal of diclofenac and ibuprofen from aqueous solution by organobentonites: Study in single and binary systems. Groundwater for Sustainable Development. 2019;8:520-529.
8. Saeid S, Tolvanen P, Kumar N, Eränen K, Peltonen J, Peurla M, et al. Advanced oxidation process for the removal of ibuprofen from aqueous solution: A non-catalytic and catalytic ozonation study in a semi-batch reactor. Applied Catalysis B: Environmental. 2018;230:77-90.
9. Rafati L, Ehrampoush MH, Rafati AA, Mokhtari M, Mahvi AH. Removal of ibuprofen from aqueous solution by functionalized strong nano-clay composite adsorbent: kinetic and equilibrium isotherm studies. Int J Environ Sci Technol (Tehran). 2017;15(3):513-524.
10. Bakr AR, Rahaman MS. Electrochemical efficacy of a carboxylated multiwalled carbon nanotube filter for the removal of ibuprofen from aqueous solutions under acidic conditions. Chemosphere. 2016;153:508-520.
11. Rahdar S, Ahmadi S. The Removal of Amoxicillin with Zno Nanoparticles in Combination with US-H2O2 Advanced Oxidation Processes from Aqueous Solutions. Iranian Journal of Health Sciences. 2019.
12. Nabiyouni G, Ghanbari D, Ghasemi J, Yousofnejad A. Microwave-assisted synthesis of MgFe2O4-ZnO nanocomposite and its photo-catalyst investigation in methyl orange degradation. Journal of Nanostructures. 2015;5(3):289-295.
13. Mehdizadeh P. Photocatalyst Ag@N/TiO2 Nanoparticles: Fabrication, Characterization, and Investigation of the Effect of Coating on Methyl Orange Dye Degradation. Journal of Nanostructures. 2017;7(3).
14. Massima Mouele ES, Tijani JO, Badmus KO, Pereao O, Babajide O, Zhang C, et al. Removal of Pharmaceutical Residues from Water and Wastewater Using Dielectric Barrier Discharge Methods—A Review. International Journal of Environmental Research and Public Health. 2021;18(4):1683.
15. Rozas O, Contreras D, Mondaca MA, Pérez-Moya M, Mansilla HD. Experimental design of Fenton and photo-Fenton reactions for the treatment of ampicillin solutions. J Hazard Mater. 2010;177(1-3):1025-1030.
16. Stan M, Lung I, Soran M-L, Leostean C, Popa A, Stefan M, et al. Removal of antibiotics from aqueous solutions by green synthesized magnetite nanoparticles with selected agro-waste extracts. Process Saf Environ Prot. 2017;107:357-372.
17. Balakrishnan RM, Ilango I, Gamana G, Bui X-T, Pugazhendhi A. Cobalt ferrite nanoparticles and peroxymonosulfate system for the removal of ampicillin from aqueous solution. Journal of Water Process Engineering. 2021;40:101823.
18. Khazri H, Ghorbel-Abid I, Kalfat R, Trabelsi-Ayadi M. Removal of ibuprofen, naproxen and carbamazepine in aqueous solution onto natural clay: equilibrium, kinetics, and thermodynamic study. Applied Water Science. 2016;7(6):3031-3040.
19. Abolhasani S, Ahmadpour A, Rohani Bastami T, Yaqubzadeh A. Facile synthesis of mesoporous carbon aerogel for the removal of ibuprofen from aqueous solution by central composite experimental design (CCD). J Mol Liq. 2019;281:261-268.
20. Guedidi H, Reinert L, Soneda Y, Bellakhal N, Duclaux L. Adsorption of ibuprofen from aqueous solution on chemically surface-modified activated carbon cloths. Arabian Journal of Chemistry. 2017;10:S3584-S3594.
21. Banerjee P, Das P, Zaman A, Das P. Application of graphene oxide nanoplatelets for adsorption of Ibuprofen from aqueous solutions: Evaluation of process kinetics and thermodynamics. Process Saf Environ Prot. 2016;101:45-53.
22. Smiljanić D, de Gennaro B, Daković A, Galzerano B, Germinario C, Izzo F, et al. Removal of non-steroidal anti-inflammatory drugs from water by zeolite-rich composites: The interference of inorganic anions on the ibuprofen and naproxen adsorption. J Environ Manage. 2021;286:112168.
23. David L, Moldovan B. Green Synthesis of Biogenic Silver Nanoparticles for Efficient Catalytic Removal of Harmful Organic Dyes. Nanomaterials. 2020;10(2):202.
24. Rafique M, Sadaf I, Rafique MS, Tahir MB. A review on green synthesis of silver nanoparticles and their applications. Artificial Cells, Nanomedicine, and Biotechnology. 2016;45(7):1272-1291.
25. Al-Senani GM, Al-Kadhi N. The Synthesis and Effect of Silver Nanoparticles on the Adsorption of Cu^{2+} from Aqueous Solutions. Applied Sciences. 2020;10(14):4840.
26. Masoumi S, Nabiyouni G, Ghanbari D. Photo-degradation of Congored, acid brown and acid violet: photo catalyst and magnetic investigation of $CuFe_2O_4$–TiO_2–Ag nanocomposites. Journal of Materials Science: Materials in Electronics. 2016;27(10):11017-11033.
27. Dhayalan M, Denison MIJ, L AJ, Krishnan K, N NG. *In vitro* antioxidant, antimicrobial, cytotoxic potential of gold and silver nanoparticles prepared using *Embelia ribes*. Nat Prod Res. 2016;31(4):465-468.
28. Moradi B, Nabiyouni G, Ghanbari D. Rapid photo-degradation of toxic dye pollutants: green synthesis of mono-disperse Fe_3O_4–CeO_2 nanocomposites in the presence of lemon extract. Journal of Materials Science: Materials in Electronics. 2018;29(13):11065-11080.
29. Yaqoob AA, Umar K, Ibrahim MNM. Silver nanoparticles: various methods of synthesis, size affecting factors and their potential applications–a review. Applied Nanoscience. 2020;10(5):1369-1378.
30. Opris R, Toma V, Olteanu D, Baldea I, Baciu AM, Lucaci FI, et

al. Effects of silver nanoparticles functionalized with *Cornus mas L*. extract on architecture and apoptosis in rat testicle. Nanomedicine. 2019;14(3):275-299.
31. Mittal AK, Chisti Y, Banerjee UC. Synthesis of metallic nanoparticles using plant extracts. Biotechnol Adv. 2013;31(2):346-356.
32. Ahmed S, Ahmad M, Swami BL, Ikram S. A review on plants extract mediated synthesis of silver nanoparticles for antimicrobial applications: A green expertise. Journal of Advanced Research. 2016;7(1):17-28.
33. Khorshidi J, Rasouli M, Rustaiee AR, Mohamadparast B. Chemical Composition of the Essential Oil of *Thymus fedtschenkoi* Growing Wild in Iran. Journal of Essential Oil Bearing Plants. 2014;17(1):173-175.
34. Rustaiee AR, Mirahmadi SF, Sefidkon F, Tabatabaei MF, Omidbaigi R. Essential Oil Content and Composition of *Thymus fedtschenkoi* Ronniger at Different Phenological Stages. Journal of Essential Oil Bearing Plants. 2011;14(5):625-629.
35. Shayganfar A, Azizi M, Rasouli M. Various strategies elicited and modulated by elevated UV-B radiation and protectant compounds in Thymus species: Differences in response over treatments, acclimation and interaction. Industrial Crops and Products. 2018;113:298-307.
36. Al-Qahtani KM. Cadmium removal from aqueous solution by green synthesis zero valent silver nanoparticles with Benjamina leaves extract. The Egyptian Journal of Aquatic Research. 2017;43(4):269-274.
37. Das R, Nath SS, Chakdar D, Gope G, Bhattacharjee R. Synthesis of silver nanoparticles and their optical properties. J Exp Nanosci. 2010;5(4):357-362.
38. Benakashani F, Allafchian AR, Jalali SAH. Biosynthesis of silver nanoparticles using Capparis spinosa L. leaf extract and their antibacterial activity. Karbala International Journal of Modern Science. 2016;2(4):251-258.
39. Hamelian M, Zangeneh MM, Amisama A, Varmira K, Veisi H. Green synthesis of silver nanoparticles using *Thymus kotschyanus* extract and evaluation of their antioxidant, antibacterial and cytotoxic effects. Appl Organomet Chem. 2018;32(9).
40. Tripathi D, Modi A, Narayan G, Rai SP. Green and cost effective synthesis of silver nanoparticles from endangered medicinal plant Withania coagulans and their potential biomedical properties. Materials Science and Engineering: C. 2019;100:152-164.
41. Esmaili N, Mohammadi P, Abbaszadeh M, Sheibani H. Green synthesis of silver nanoparticles using *Eucalyptus comadulensis* leaves extract and its immobilization on magnetic nanocomposite (GO-Fe_3O_4/PAA/Ag) as a recoverable catalyst for degradation of organic dyes in water. Appl Organomet Chem. 2020;34(4).
42. Rajeshkumar S, Bharath LV. Mechanism of plant-mediated synthesis of silver nanoparticles – A review on biomolecules involved, characterisation and antibacterial activity. Chemico-Biological Interactions. 2017;273:219-227.
43. Del Vecchio P, Haro NK, Souza FS, Marcílio NR, Féris LA. Ampicillin removal by adsorption onto activated carbon: kinetics, equilibrium and thermodynamics. Water Sci Technol. 2019;79(10):2013-2021.
44. Wang G, Wu T, Li Y, Sun D, Wang Y, Huang X, et al. Removal of ampicillin sodium in solution using activated carbon adsorption integrated with H_2O_2 oxidation. Journal of Chemical Technology & Biotechnology. 2011;87(5):623-628.
45. Phasuphan W, Praphairaksit N, Imyim A. Removal of ibuprofen, diclofenac, and naproxen from water using chitosan-modified waste tire crumb rubber. J Mol Liq. 2019;294:111554.
46. Lung I, Soran M-L, Stegarescu A, Opris O, Gutoiu S, Leostean C, et al. Evaluation of CNT-COOH/MnO_2/Fe_3O_4 nanocomposite for ibuprofen and paracetamol removal from aqueous solutions. J Hazard Mater. 2021;403:123528.
47. Saxena M, Sharma N, Saxena R. Highly efficient and rapid removal of a toxic dye: Adsorption kinetics, isotherm, and mechanism studies on functionalized multiwalled carbon nanotubes. Surfaces and Interfaces. 2020;21:100639.
48. Zaheer Z, AbuBaker Bawazir W, Al-Bukhari SM, Basaleh AS. Adsorption, equilibrium isotherm, and thermodynamic studies to the removal of acid orange 7. Materials Chemistry and Physics. 2019;232:109-120.
49. Simonin J-P. On the comparison of pseudo-first order and pseudo-second order rate laws in the modeling of adsorption kinetics. Chem Eng J. 2016;300:254-263.
50. Kebede TG, Dube S, Nindi MM. Application of mesoporous nanofibers as sorbent for removal of veterinary drugs from water systems. Sci Total Environ. 2020;738:140282.
51. Marinescu L, Ficai D, Oprea O, Marin A, Ficai A, Andronescu E, et al. Optimized Synthesis Approaches of Metal Nanoparticles with Antimicrobial Applications. Journal of Nanomaterials. 2020;2020:1-14.
52. Choong CE, Ibrahim S, Basirun WJ. Mesoporous silica from batik sludge impregnated with aluminum hydroxide for the removal of bisphenol A and ibuprofen. Journal of Colloid and Interface Science. 2019;541:12-17.
53. Nourmoradi H, Moghadam KF, Jafari A, Kamarehie B. Removal of acetaminophen and ibuprofen from aqueous solutions by activated carbon derived from Quercus Brantii (Oak) acorn as a low-cost biosorbent. Journal of Environmental Chemical Engineering. 2018;6(6):6807-6815.